

Large-scale shell-model study of 2ν ECEC process in ^{78}Kr

Deepak Patel, Praveen C. Srivastava

Department of Physics, Indian Institute of Technology Roorkee, Roorkee 247 667, India

Abstract.

In this work, we present the systematic study of 2ν ECEC process in the ^{78}Kr using large-scale shell-model calculations with the GWBXC effective interaction. We first validate the efficiency of the utilized interaction by comparing the theoretical low-lying energy spectra, the kinematic moment of inertia, and reduced transition probabilities with the experimental data for both the parent and grand-daughter nuclei ^{78}Kr and ^{78}Se , respectively. Additionally, we examine the shell-model level densities of the 1^+ states in the intermediate nucleus ^{78}Br , comparing them with the predictions from the Back-shifted Fermi gas model. We analyze the variation of cumulative nuclear matrix elements (NMEs) for the 2ν ECEC process in ^{78}Kr as a function of 1^+ state energies in the intermediate nucleus ^{78}Br up to the saturation level. Our estimated half-life for ^{78}Kr , extracted from the shell-model predicted NMEs, shows good agreement with the experimental value. The Gamow-Teller transitions from the lowest 1^+ state of ^{78}Br via both the $\text{EC}+\beta^+$ and β^- -channels are also discussed.

1. Introduction

Double electron capture (ECEC) is one of the rarest weak interaction processes and has been a subject of significant interest in the field of nuclear and particle physics over the last few decades [1, 2, 3, 4, 5, 6, 7, 8, 9, 10, 11, 12, 13, 14, 15, 16, 17]. This process involves the simultaneous capture of two electrons by a nucleus and can occur in two distinct modes: two-neutrino double electron capture (2ν ECEC) and neutrinoless double electron capture (0ν ECEC) [8]. These modes are represented by the reactions $(Z, A) + 2e^- \rightarrow (Z - 2, A) + 2\nu_e$ for 2ν ECEC and $(Z, A) + 2e^- \rightarrow (Z - 2, A)$ for 0ν ECEC [13]. The ECEC process primarily takes place in those nuclei where single β^+ /EC process is either energetically forbidden or significantly suppressed. The 2ν ECEC process adheres to all conservation laws of the standard model. However, the 0ν ECEC, which is not observed yet, violates lepton number conservation, providing key insights into the Majorana nature of neutrinos and physics beyond the standard model [18, 19, 20]. In this study, we consider only the 2ν ECEC process, which is essential for probing nuclear structure and accessing the effective value of weak axial-vector coupling constant.

The ECEC process is the less explored counterpart of the double beta-minus decay due to its longer half-lives and lower Q-values, which pose significant challenges for experimental detection [15]. Despite this, the 2ν ECEC process has been observed in three nuclei ^{78}Kr [1, 2], ^{124}Xe [9, 10], and ^{130}Ba [15, 21]. There are other prominent candidates of the 2ν ECEC process, such as ^{126}Xe and ^{132}Ba , but only lower limits of their half-lives can be observed so far [13, 15, 22]. In these circumstances, the theoretical and experimental investigation of the 2ν ECEC process in the above nuclei becomes crucial. For ^{78}Kr , the well-known candidate of 2ν ECEC process, the half-life has been experimentally measured in two different experiments as $[9.2_{-2.6}^{+5.5}(\text{stat}) \pm 1.3(\text{syst})] \times 10^{21}$ yr using a copper low-background proportional counter [1], and $[1.9_{-0.7}^{+1.3}(\text{stat}) \pm 0.3(\text{syst})] \times 10^{22}$ yr using the time-resolving current pulse from the large low-background proportional counter (LPC) [2]. Therefore, it is essential to assess the effectiveness of various nuclear models in calculating the 2ν ECEC nuclear matrix element (NME) for ^{78}Kr , which plays an important role in determining the accurate half-life.

In recent decades, various theoretical approaches, including the quasiparticle random-phase approximation (QRPA), the interacting boson model (IBM), the Hartree-Fock-Bogoliubov model (HFB), and the nuclear shell model (NSM) have been employed to study $\beta^-\beta^-$, $\beta^+\beta^+$, $\beta^+\text{EC}$, and ECEC processes [23, 24, 25, 26, 27, 28, 29, 30, 31]. The nuclear shell model is a widely adopted theoretical framework for studying the nuclear structure and decay processes. Several calculations have been performed to determine the NMEs for $\beta^-\beta^-$ decay using the shell-model [12, 29, 30, 32, 33, 34, 35, 36], while the 2ν ECEC process has been less explored within this framework. With new advancements in computational capabilities, it is now feasible to accurately estimate the 2ν ECEC NME by including a large number of 1^+ states in the intermediate nucleus for this decay process. For a precise prediction of the NME, it is crucial to ensure that the employed model space can sustain the level density of 1^+ states in the intermediate nucleus across the relevant energy range. In this context, the efficiency of the effective interaction and model space can be evaluated by comparing the level density of these 1^+ states with that predicted by simple nuclear level density models, such as the Back-shifted Fermi gas model (BFM) [37, 38].

Motivated by the recent experimental data on 2ν ECEC studies [1, 2] and advancements in the computational techniques, we have conducted large-scale shell-model calculations to investigate the 2ν ECEC process in ^{78}Kr . The primary goal of this study is to determine a precise value for the 2ν ECEC NME in ^{78}Kr and provide an accurate prediction of the half-life close to the experimental value. Additionally, we aim to examine the level density of 1^+ states in the intermediate nucleus ^{78}Br and explore the variation in cumulative NME with respect to the energy of these 1^+ states.

This paper is organized as follows: Section 2 provides a brief overview of the theoretical framework used to calculate the 2ν ECEC NME and half-life, along with the effective shell-model interaction employed in this work. In Section 3, we present the spectroscopic properties of the parent (^{78}Kr) and grand-daughter (^{78}Se) nuclei, the

level density of 1^+ states in the ^{78}Br , the variation of cumulative NME, the estimated half-life of ^{78}Kr for the 2ν ECEC process using the final cumulative NME, the role of Gamow-Teller (GT) transitions from the lowest 1^+ state of ^{78}Br via both the $\text{EC}+\beta^+$ and β^- -channels and their partial half-lives. Finally, Section 4 summarizes the outcomes and draws the conclusions.

2. Theoretical Framework

2.1. Half-life

The half-life for the 2ν ECEC process can be given as follows

$$T_{1/2}^{2\nu} = \frac{1}{G_{2\nu}^{\text{ECEC}} (g_A^{\text{eff}})^4 |M_{2\nu}|^2}, \quad (1)$$

where $G_{2\nu}^{\text{ECEC}}$ [11, 39] represents the phase-space factor and g_A^{eff} corresponds to effective axial-vector coupling constant [40]. The NME $M_{2\nu}$ for 2ν ECEC process is given by [41, 42]

$$M_{2\nu} = \sum_k \frac{\langle 0_{\text{g.s.}}^{(f)} || \sigma\tau^+ || 1_k^+ \rangle \langle 1_k^+ || \sigma\tau^+ || 0_{\text{g.s.}}^{(i)} \rangle}{[\frac{1}{2}Q_{\text{ECEC}} + E(1_k^+) - M_i]/m_e + 1}. \quad (2)$$

Here, $E(1_k^+) - M_i$ represents the energy difference between the k^{th} intermediate 1^+ state and the ground state (g.s.) of the initial nucleus; m_e denotes the rest mass of the electron; $0_{\text{g.s.}}^{(i)}$ ($0_{\text{g.s.}}^{(f)}$) corresponds the ground state of the initial (final) nuclei; σ stands for the pauli matrix; τ^+ represents the isospin raising operator. Q_{ECEC} (Q -value) signifies the energy released during the process. $\langle 0_{\text{g.s.}}^{(f)} || \sigma\tau^+ || 1_k^+ \rangle$ (or $\langle 1_k^+ || \sigma\tau^+ || 0_{\text{g.s.}}^{(i)} \rangle$) refers the reduced GT matrix element. It is important to note that within the shell-model framework, the effective axial-vector coupling constant, g_A^{eff} , in Eq. (1) arises from the effective renormalization of the spin-isospin operator $\sigma\tau^+$ in the NME of Eq. (2). By factoring g_A^{eff} outside the squared NME in Eq. (1), the $M_{2\nu}$ in Eq. (2) becomes independent of the effective axial coupling.

2.2. Model space and Hamiltonian

The shell-model Hamiltonian can be represented as follows

$$H = \sum_{\alpha} \varepsilon_{\alpha} \hat{N}_{\alpha} + \frac{1}{4} \sum_{\alpha\beta\delta\gamma J} \langle j_{\alpha} j_{\beta} | V | j_{\gamma} j_{\delta} \rangle_J \times O_{J;j_{\alpha} j_{\beta}}^{\dagger} O_{J;j_{\delta} j_{\gamma}}, \quad (3)$$

where, $\alpha = \{nlj\}$ stands for the single-particle orbitals and ε_{α} denote the corresponding single-particle energies. \hat{N}_{α} corresponds the particle number operator. $\langle j_{\alpha} j_{\beta} | V | j_{\gamma} j_{\delta} \rangle_J$ refers two-body matrix element. O_J^{\dagger} , and O_J are the fermion pair creation and annihilation operators, respectively.

The GWBXXG effective interaction [43, 44, 45, 46] is utilized for calculating the reduced GT matrix elements. The mean-field part of the shell-model Hamiltonian corresponding to the GWBXXG interaction consists of $0f_{5/2}1p0g_{9/2}$ proton and

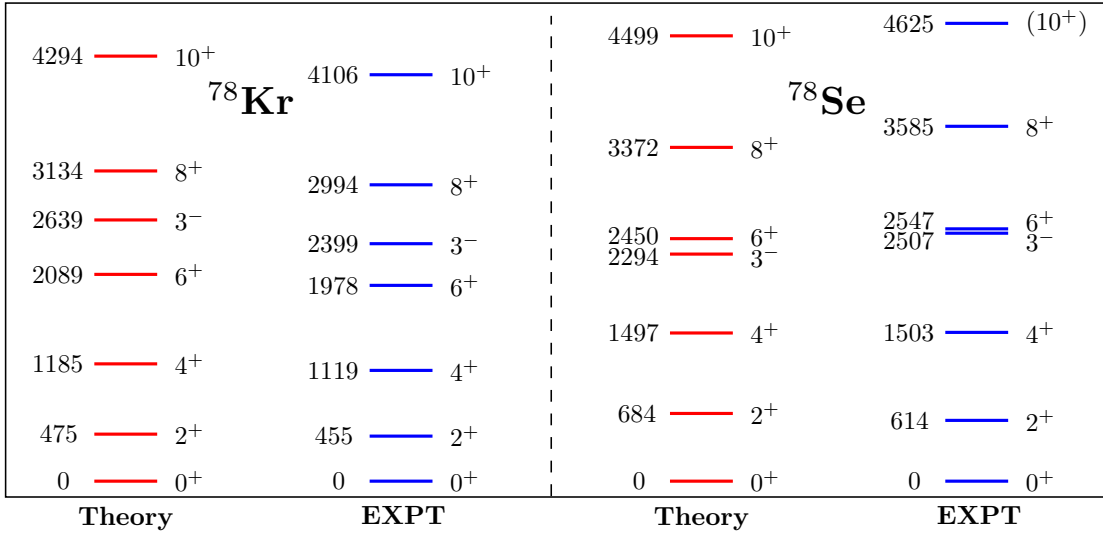


Figure 1. Comparison between the theoretical and experimental [51] energy levels in the parent (^{78}Kr) and grand-daughter (^{78}Se) nuclei.

$1p_{1/2}0g_{1d_{2s}}$ neutron orbitals. Previously, this interaction has been employed to investigate the structure of different nuclei [47, 48, 49]. We have also used this interaction in our recent study on $2\nu\beta^-\beta^-$ -decay [50]. It is not possible to perform our calculations in the full model space due to the huge shell-model dimensions. Thus, we have employed truncations by completely restricting neutron excitation across $N = 50$ shell and allowed the neutrons to fill in the $1p_{1/2}$ and $0g_{9/2}$ orbitals only. To ensure the saturation level in the cumulative NMEs, we have considered 5000 1^+ states in the intermediate nucleus ^{78}Br for GT transitions. The shell-model code NuShellX [52] has been utilized in the diagonalization of the shell-model Hamiltonian matrices.

3. Results and Discussions

In this section, we present the shell-model calculated results for the 2ν ECEC process in ^{78}Kr . We first compare the calculated spectroscopic properties, including the low-lying energy spectra, kinematic moment of inertia, and reduced quadrupole transition probabilities, in the ^{78}Kr and the ^{78}Se nuclei with the corresponding experimental data. Next, we discuss the shell-model level densities of the 1^+ states in the ^{78}Br and compare them with the predictions from the BFM. We also analyze the variation of the cumulative NME for the 2ν ECEC process in ^{78}Kr as a function of the 1^+ state energies in ^{78}Br and estimate the half-life using the final cumulative NME. Finally, we briefly discuss the GT transitions from the lowest 1^+ state of ^{78}Br via both the $\text{EC}+\beta^+$ and β^- -channels.

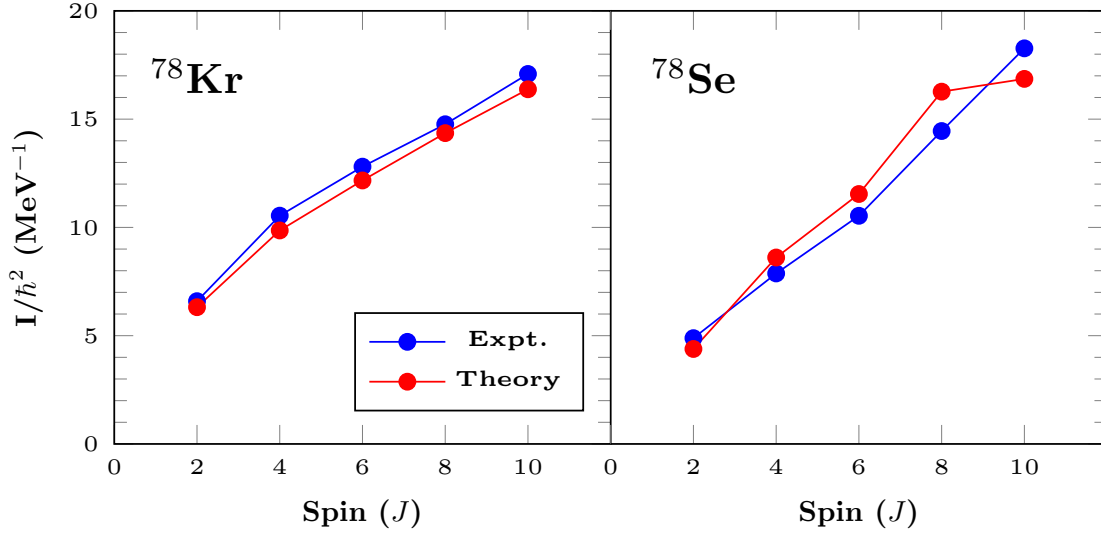


Figure 2. Comparison of the theoretical and experimental kinematic moment of inertia with respect to yrast positive-parity spins.

Table 1. Comparison of the theoretical and experimental $B(E2)$ strengths (in Weisskopf unit (W.u.)) [53] in the parent and grand-daughter nuclei of 2ν ECEC process. The effective charges are taken as $e_\pi = 1.7e, e_\nu = 1.1e$ [54].

Isotope	$J_i^\pi \rightarrow J_f^\pi$	Theory	Expt.
^{78}Kr	$2_1^+ \rightarrow 0_1^+$	43.3	67.9(22)
	$4_1^+ \rightarrow 2_1^+$	62.5	88(5)
	$6_1^+ \rightarrow 4_1^+$	68.2	94(11)
	$8_1^+ \rightarrow 6_1^+$	67.5	≈ 85
	$10_1^+ \rightarrow 8_1^+$	63.8	80(12)
^{78}Se	$2_1^+ \rightarrow 0_1^+$	28.3	33.5(8)
	$4_1^+ \rightarrow 2_1^+$	38.6	49.5(24)
	$6_1^+ \rightarrow 4_1^+$	38.4	47(14)
	$8_1^+ \rightarrow 6_1^+$	33.9	56(19)
	$10_1^+ \rightarrow 8_1^+$	42.7	-

3.1. Spectroscopic properties

It is required to test the efficiency of the present effective interaction before calculating 2ν ECEC NME in ^{78}Kr . For this, we have compared the shell-model calculated low-lying energy spectra, kinematic moment of inertia (see Figs. 1 and 2) and reduced quadrupole transition probabilities between the yrast states (see Table 1) in the ^{78}Kr and ^{78}Se with the experimental data.

It is clear from Fig. 1 that the present effective interaction successfully reproduces the low-lying yrast states in the ^{78}Kr and ^{78}Se . Shell-model calculations predict that the $0^+ - 6^+$ states in ^{78}Kr are primarily dominated by the $\pi(f_{5/2}^4 p_{3/2}^2 g_{9/2}^2) \otimes \nu(g_{9/2}^4)$ and

$\pi(f_{5/2}^2 p_{3/2}^4 g_{9/2}^2) \otimes \nu(g_{9/2}^4)$ configurations. A smaller but notable contribution from the $\pi(f_{5/2}^3 p_{3/2}^3 g_{9/2}^2) \otimes \nu(g_{9/2}^4)$ configuration also comes in the above states, which becomes the most dominating component in the $8^+ - 10^+$ states. The dominance of the $\pi(g_{9/2})$ orbital in the low-lying structure of ^{78}Kr indicates that the high- j proton orbital $g_{9/2}$ intrudes into the pf -shell region near the Fermi surface. In the other case, the $0^+ - 8^+$ states in ^{78}Se are mainly characterized by the $\pi(f_{5/2}^4 p_{3/2}^2) \otimes \nu(g_{9/2}^6)$ configuration and proton excitations in the $g_{9/2}$ orbital play less significant role. However, for the 10^+ state, a proton-pair excitation in the $g_{9/2}$ orbital is found, with major components from the $[\pi(f_{5/2}^3 p_{3/2}^1 g_{9/2}^2) \otimes \nu(g_{9/2}^6) \sim 21.0\%]$, $[\pi(f_{5/2}^2 p_{3/2}^2 g_{9/2}^2) \otimes \nu(g_{9/2}^6) \sim 19.7\%]$, and $[\pi(f_{5/2}^4 g_{9/2}^2) \otimes \nu(g_{9/2}^6) \sim 19.3\%]$ configurations.

The kinematic moment of inertia (I/\hbar^2) is an important quantity to describe the rotational behavior of a band. In Fig. 2, we have shown the variation of theoretical and experimental kinematic moments of inertia in ^{78}Kr and ^{78}Se as a function of yrast positive-parity spins. The relation $I/\hbar^2 = (2J - 1)/E_\gamma(J \rightarrow J - 2)$ is used, where E_γ represents the energy difference between two consecutive states in the g.s. band, which are at the spin difference of $\Delta J = 2$. Our theoretical results show quite good agreement with the experimental data, particularly for ^{78}Kr , compared to the previous study [55].

As reported in Table 1, the calculated $B(E2)$ strengths for both the ^{78}Kr and ^{78}Se are slightly lower but consistent with the experimental data [53]. Although if we incorporate the neutron orbitals $0g_{7/2}1d_{2s}$ in our model space with $1p - 1h$ excitation across $N = 50$, then it is possible to improve the $B(E2)$ strengths, but these orbitals cannot be included in the current study due to the computational limitations for the 2ν ECEC NME calculation with higher 1^+ state energies in the ^{78}Br . Nevertheless, the shell-model predicted energy spectra, kinematic moment of inertia, and $B(E2)$ strengths show quite reasonable agreement with the experimental data for both nuclei. Thus, the present effective interaction can be reliably used to calculate the 2ν ECEC NME in this study.

3.2. Level density of 1^+ states

The Bethe formula for level density [37], incorporating spin dependence within the BFM, can be expressed as [38]

$$\rho(U, J) = \rho(U) \cdot f(J), \quad (4)$$

where

$$\rho(U) = \frac{1}{12\sqrt{2}\sigma} \frac{e^{2\sqrt{aU}}}{a^{1/4}U^{5/4}}, \quad (5)$$

and

$$f(J) = \frac{(2J + 1)e^{-(J+\frac{1}{2})^2/2\sigma^2}}{2\sigma^2}. \quad (6)$$

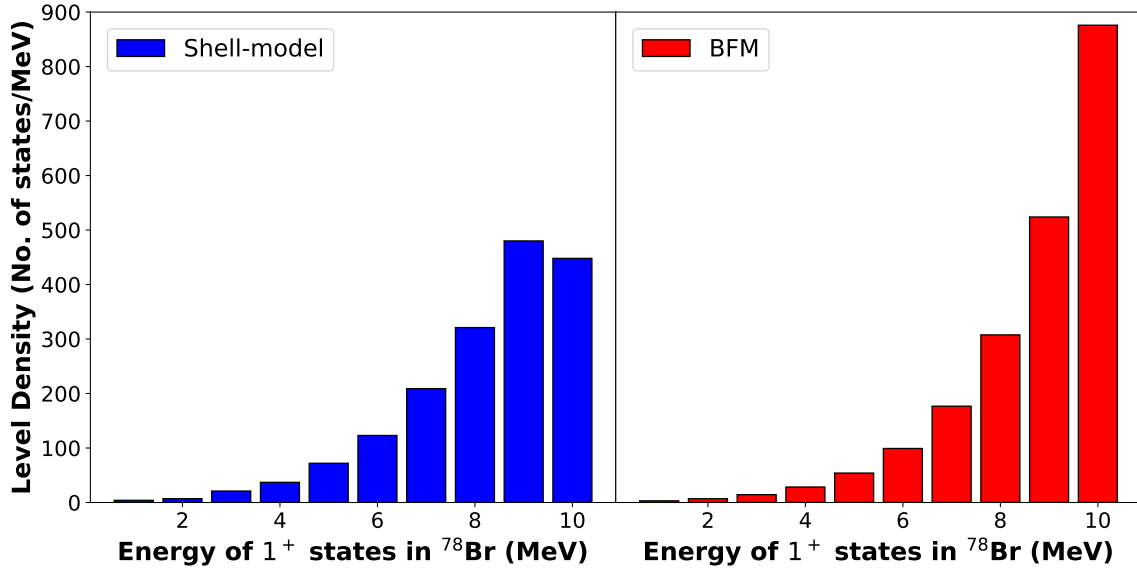


Figure 3. Comparison between the shell-model and BFM calculated level-densities of 1^+ states in ^{78}Br .

In this formulation, the spin cutoff parameter [38] is described as $\sigma^2 = 0.0888A^{2/3}\sqrt{a(E - \delta)}$. The level density parameter a is defined as $a = (A/16) \text{ MeV}^{-1}$ [56], and $U = (E - \delta)$ [57], where E is the excitation energy for a given spin state J , and A represents the atomic mass. The back-shifted parameter δ (in MeV) is determined by the following expression [58]

$$\delta = \begin{cases} 12/\sqrt{A}, & \text{for even - even nuclei} \\ 0, & \text{for odd - } A \text{ nuclei} \\ -12/\sqrt{A}, & \text{for odd - odd nuclei.} \end{cases} \quad (7)$$

By accounting for equiparity distribution, the level density can be represented as follows [57]

$$\rho(U, J, \pi) = \frac{1}{2}\rho(U) \cdot f(J). \quad (8)$$

Fig. 3 depicts the comparison of the shell-model calculated level density of 1^+ states in ^{78}Br with the BFM predicted level density for odd-odd nuclei with $A = 78$ (using Eq. (8)). It is clear from Fig. 3 that the shell-model level densities of 1^+ states in ^{78}Br are consistent with the BFM predictions up to approximately 9 MeV. Therefore, the cumulative NME contribution for the 2ν ECEC process in ^{78}Kr is expected to be well captured by shell-model calculations up to this energy. Beyond 9 MeV, some contributions to the cumulative NME may be missed by the shell-model calculations but will be significant in the final value of $|M_{2\nu}|$ only if the cumulative NME has not yet reached the saturation level. The inclusion of further neutron and proton orbitals in the model space can extend the energy range to sustain the level density of the 1^+ state in ^{78}Br by shell-model with more advanced computational facilities, which is the future work.

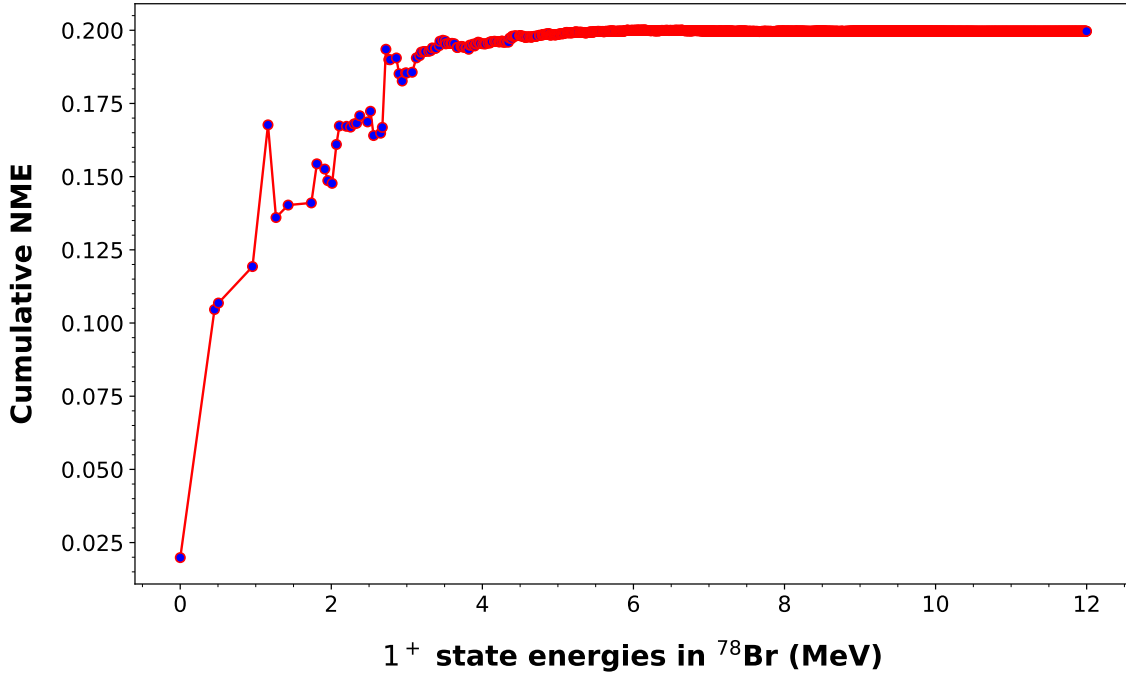


Figure 4. Variation of the cumulative NME with respect to the 1^+ state energies in the intermediate nucleus ^{78}Br .

Table 2. Shell-model calculated 2ν ECEC NMEs and the extracted half-lives.

Nucleus	$ M_{2\nu} $	$G_{2\nu}^{\text{ECEC}}$ (yr^{-1}) [11]	g_A^{eff}	Calculated $T_{1/2}^{2\nu}$ (yr)	Experimental value of $T_{1/2}^{2\nu}$ (yr)
^{78}Kr	0.1997	520.518×10^{-24}	1.27- 1.00	$(1.85-4.82) \times 10^{22}$	$[9.2_{-2.6}^{+5.5}(\text{stat}) \pm 1.3(\text{syst})] \times 10^{21}$ [1] $[1.9_{-0.7}^{+1.3}(\text{stat}) \pm 0.3(\text{syst})] \times 10^{22}$ [2]

3.3. Variation of cumulative NME and half-life

Here, we analyze the variation in the shell-model predicted cumulative NME for the 2ν ECEC process in ^{78}Kr and compare the half-life, calculated from the final NME (using Eq. 1) with the available experimental data. Accurate determination of the NME is essential for the estimation of precise half-life. Fig. 4 depicts the variation of cumulative NME as a function of the 1^+ state energies in the ^{78}Br , up to the saturation level. In the present calculation, the excitation energies of the 1^+ states in ^{78}Br are shifted so that the lowest 1^+ state comes at the experimental energy of 0 MeV. The Q_{ECEC} value is taken from the Ref. [11]. The lowest 1^+ state in ^{78}Br contributes 9.95% to the final NME. After several significant constructive and destructive contributions, likely within the 0-5 MeV range, the cumulative NME begins to saturate approximately near the 8 MeV, with a final value of 0.1997. It is important to mention that since

the cumulative NME nearly saturates before the energy range where our model space becomes less efficient in sustaining the level density of the 1^+ states in ^{78}Br . Thus, it has minimal effect on the final NME value. In Fig. 4, the cumulative NME is presented up to 12 MeV, accounting for 2320 1^+ states in ^{78}Br , as it has already saturated at the lower energies.

The estimated half-life compared to the experimental data is presented in Table 2. The experimental half-lives reported in Table 2 are corresponding to the electron captures from the K-shell pairs. Therefore, we use the $G_{2\nu}^{\text{ECEC}} = 661.9 \times 0.7864 \times 10^{-24} \text{ yr}^{-1}$ [11] in our calculations, which is appropriate for the $2\nu\text{KK}$ mode. We have considered a range of g_A^{eff} from $g_A^{\text{free}} = 1.27$ to a quenched value of $g_A^{\text{quen}} = 1.00$. The calculated half-life using the shell-model predicted NME shows quite reasonable agreement with the experimental results [1, 2]. Previously, Romyantsev *et al.* [59] calculated the $2\nu\text{ECEC}$ NME for ^{78}Kr as 0.0146 using the BCS and the pair-vibration models, a small value that contributed to a larger half-life prediction compared to the experimental data. However, recent half-life measurement has yielded an NME for the $2\nu\text{ECEC}$ process in ^{78}Kr of $0.318_{-0.073}^{+0.100}$ [2, 11], which is approximately 1.6 times larger than the NME obtained in the present study. In the future, it may be possible to achieve more accurate NME from theoretical calculations with a larger model space using advanced computational resources.

3.4. GT transitions from the lowest 1^+ state of the ^{78}Br

Experimentally, the GT transitions from the lowest 1^+ state in the ^{78}Br can occur through both the $\text{EC}+\beta^+$ and β^- -decay channels. However, only limits on the branching ratios (*B.R.*) for the $^{78}\text{Br}(1_1^+) \rightarrow ^{78}\text{Se}(0^+, 2^+)$ and $^{78}\text{Br}(1_1^+) \rightarrow ^{78}\text{Kr}(2_1^+)$ transitions are known, with values of $\geq 99.99\%$ and $\leq 0.01\%$, respectively [51, 60]. As reported in Ref. [60], the dominant contribution (99.7%) to the $\text{EC}+\beta^+$ decay path arises from the $^{78}\text{Br}(1_1^+) \rightarrow ^{78}\text{Se}(0_{\text{g.s.}}^+)$ and $^{78}\text{Br}(1_1^+) \rightarrow ^{78}\text{Se}(2_1^+)$ transitions. By considering only these two transitions for the $\text{EC}+\beta^+$ channel and the $^{78}\text{Br}(1_1^+) \rightarrow ^{78}\text{Kr}(2_1^+)$ transition for the β^- -channel in our shell-model calculations, we obtain a total half-life of 56.34 min for the 1_1^+ state in ^{78}Br . This value is of the same order as the experimental half-life (6.45(4) min [51]) but approximately 8.7 times larger. The partial half-lives for the $^{78}\text{Br}(1_1^+) \rightarrow ^{78}\text{Se}(0_{\text{g.s.}}^+)$, $^{78}\text{Br}(1_1^+) \rightarrow ^{78}\text{Se}(2_1^+)$, and $^{78}\text{Br}(1_1^+) \rightarrow ^{78}\text{Kr}(2_1^+)$ transitions are calculated as 58.34, 1863.32, and 13394.14 min, respectively. The branching ratio for the combined transitions $^{78}\text{Br}(1_1^+) \rightarrow ^{78}\text{Se}(0_{\text{g.s.}}^+)$ (96.56%) and $^{78}\text{Br}(1_1^+) \rightarrow ^{78}\text{Se}(2_1^+)$ (3.02%) is 99.58%. While, the remaining 0.42% is attributed to the $^{78}\text{Br}(1_1^+) \rightarrow ^{78}\text{Kr}(2_1^+)$ transition. These *B.R.* are close to the experimental limits. An analogous situation has also been found in the case of $\beta^-\beta^-$ -decay of ^{100}Mo [51, 61]. The estimated partial half-lives are corresponding to the $g_A^{\text{eff}} = 1.00$. Although the *B.R.* remain unaffected by changing the g_A^{eff} . The total half-life for the 1_1^+ state in ^{78}Br is calculated as 34.93 min with $g_A^{\text{free}} = 1.27$, which aligns more closely with the experimental value than corresponding to the $g_A^{\text{eff}} = 1.00$. This improvement is also reflected in the calculated half-life for the

2ν ECEC process, as shown in Table 2. Therefore, our nuclear model, which accurately estimates the half-life of the 1_1^+ state in ^{78}Br , is also likely to yield a precise prediction of the half-life for the 2ν ECEC process in ^{78}Kr . These analyses support the dominance of this 1_1^+ state in contributing to the 2ν ECEC process.

The partial half-lives are calculated using the formula $t_{1/2}^{(n)} = \kappa / (f_0 B_{\text{GT}}^{(n)})$ [62]. Here, n stands for the different GT transitions; κ denotes the universal constant, which equals to 6289 s [63]; $B_{\text{GT}}^{(n)}$ denotes the GT reduced transition probability and given in terms of reduced GT matrix elements $\langle J_f || \sigma \tau^\pm || J_i \rangle$ as follows [64]

$$B_{\text{GT}} = \frac{(g_A^{\text{eff}})^2}{2J_i + 1} |\langle J_f || \sigma \tau^\pm || J_i \rangle|^2, \quad (9)$$

where $J_i(J_f)$ is spin of the initial (final) state. The f_0 is the phase-space factor and can be written for β^\pm -decay as follows [65]

$$f_0^{(\pm)} = \int_1^{E_0} F_0(\mp Z_f, \epsilon) p \epsilon (E_0 - \epsilon)^2 d\epsilon. \quad (10)$$

Here, F_0 denotes the Fermi function; Z_f stands for the atomic number of the final nucleus. The other parameters can be given by

$$\epsilon = \frac{E_e}{m_e c^2}, \quad E_0 = \frac{E_i - E_f}{m_e c^2}, \quad p = \sqrt{\epsilon^2 - 1} = \frac{p_e c}{m_e c^2}, \quad (11)$$

where, E_e represents the total energy of the emitted positron/electron and $E_i(E_f)$ denotes the energy of the initial (final) nuclear state.

The phase-space factor for electron capture (EC) can be written as [64]

$$f_0^{(EC)} = 2\pi(\alpha Z_i)^3 (\epsilon_0 + E_0)^2, \quad (12)$$

where, $\epsilon_0 = 1 - [(\alpha Z_i)^2]/2$, and the fine-structure constant, $\alpha \approx 1/137$; Z_i denotes the atomic number of initial nucleus.

Finally, we have calculated the total half-life and $B.R.$ using the following expressions [64]

$$\frac{1}{T_{1/2}^{\text{total}}} = \sum_j \frac{1}{t_{1/2}^{(j)}}; \quad B.R.^{(n)} = T_{1/2}^{\text{total}} / t_{1/2}^{(n)}. \quad (13)$$

Here, it is important to mention that when we consider only the single transitions $^{78}\text{Br}(1_1^+) \rightarrow ^{78}\text{Se}(0_{\text{g.s.}}^+)$ for the $\text{EC} + \beta^+$ decay and $^{78}\text{Br}(1_1^+) \rightarrow ^{78}\text{Kr}(0_{\text{g.s.}}^+)$ for the β^- -decay, the resulting partial half-lives corresponding to $g_A^{\text{free}} = 1.27$ are 36.17 min for the $\text{EC} + \beta^+$ channel and 254.21 min for the β^- -channel. In this case, the calculated $B.R.$ (87.54% for the $\text{EC} + \beta^+$ channel and 12.46% for the β^- -channel) show some deviations from the experimental limits, which may pose a smaller effect on the accuracy of the calculated NME.

4. Summary and conclusion

In this study, we have conducted large-scale shell-model calculations to compute a precise NME for the 2ν ECEC process in the ^{78}Kr , utilizing the GWBXXG effective interaction. To validate the efficiency of this interaction, we first calculated the spectroscopic properties, such as energy spectra, kinematic moment of inertia, and reduced quadrupole transition probabilities for the parent (^{78}Kr) and grand-daughter (^{78}Se) nuclei, as well as the level density of 1^+ states in the intermediate nucleus ^{78}Br . Our results exhibit quite remarkable agreement with the experimental data, especially in the low-lying energy spectra and kinematic moment of inertia. The model space effectively captures the level density of the 1^+ states in ^{78}Br up to 9 MeV, though some deviation occurs when compared to the predicted level density from the BFM at higher energies. Analyzing the cumulative NME as a function of 1^+ state energies in the ^{78}Br revealed that the cumulative NMEs start to saturate around 8 MeV, indicating that our model space successfully incorporates the significant contributions to the final cumulative NME. Based on the computed NME, we have estimated the half-life of ^{78}Kr for the 2ν ECEC process corresponding to the electron captures from the K-shell pairs, which shows quite reasonable agreement with the experimental data. The role of GT transitions for the 2ν ECEC process in ^{78}Kr from the lowest 1^+ state of ^{78}Br via both the $\text{EC}+\beta^+$ and β^- -channels is also briefly discussed. We will explore the 2ν ECEC process in the ^{78}Kr and other candidates with larger model spaces to get more accurate NME in the future once the new computational facilities allow us to do so.

Acknowledgments

We are thankful for the financial support provided by MHRD, the Government of India, and SERB (India), CRG/2022/005167. We would like to acknowledge the National Supercomputing Mission (NSM) for providing computing resources of ‘PARAM Ganga’ at the IIT Roorkee, implemented by C-DAC and supported by the Ministry of Electronics and Information Technology (MeitY) and Department of Science and Technology (DST), Government of India.

References

- [1] Yu. M. Gavriluk, A. M. Gangapshev, V. V. Kazalov, V. V. Kuzminov, S. I. Panasenko, and S. S. Ratkevich, Indications of $2\nu 2K$ capture in ^{78}Kr , *Phys. Rev. C* **87**, 035501 (2013).
- [2] S. S. Ratkevich, A. M. Gangapshev, Yu. M. Gavriluk, F. F. Karpeshin, V. V. Kazalov *et al.*, Comparative study of the double- K -shell-vacancy production in single- and double-electron-capture decay, *Phys. Rev. C* **96**, 065502 (2017).
- [3] J. Suhonen, Double beta decays of ^{124}Xe investigated in the QRPA framework, *J. Phys. G: Nucl. Part. Phys.* **40**, 075102 (2013).
- [4] P. Pirinen and J. Suhonen, Systematic approach to β and $2\nu\beta\beta$ decays of mass $A = 100 - 136$ nuclei, *Phys. Rev. C* **91**, 054309 (2015).

- [5] E. A. Coello Pérez, J. Menéndez, and A. Schwenk, Two-neutrino double electron capture on ^{124}Xe based on an effective theory and the nuclear shell model, *Phys. Lett. B* **797**, 134885 (2019).
- [6] O. Nițescu, S. Ghinescu, V.-A. Sevestrean, M. Horoi, F. Šimkovic, and S. Stoica, Theoretical analysis and predictions for the double electron capture of ^{124}Xe , *J. Phys. G: Nucl. Part. Phys.* **51**, 125103 (2024).
- [7] S. Mishra, A. Shukla, R. Sahu, and V. K. B. Kota, Deformed shell model calculations of half lives for β^+ /EC decay and $2\nu\beta^+\beta^+/\beta^+\text{EC}/\text{ECEC}$ decay in medium-heavy $N \sim Z$ nuclei, *Phys. Rev. C* **78**, 024307 (2008).
- [8] E. Aprile, J. Aalbers, F. Agostini, M. Alfonsi, F. D. Amaro *et al.* (XENON Collaboration), Search for two-neutrino double electron capture of ^{124}Xe with XENON100, *Phys. Rev. C* **95**, 024605 (2017).
- [9] E. Aprile, K. Abe, F. Agostini, S. A. Maouloud, M. Alfonsi *et al.* (XENON Collaboration), Double-weak decays of ^{124}Xe and ^{136}Xe in the XENON1T and XENONnT experiments, *Phys. Rev. C* **106**, 024328 (2022).
- [10] E. Aprile, J. Aalbers, F. Agostini, M. Alfonsi, L. Althueser *et al.* (XENON Collaboration), Observation of two-neutrino double electron capture in ^{124}Xe with XENON1T, *Nature* **568**, 532 (2019).
- [11] O. Nițescu, S. Ghinescu, S. Stoica, and F. Šimkovic, A Systematic Study of Two-Neutrino Double Electron Capture, *Universe* **10**, 98 (2024).
- [12] D. Patel, P. C. Srivastava, V. K. B. Kota, and R. Sahu, Large-scale shell-model study of two-neutrino double beta decay of ^{82}Se , ^{94}Zr , ^{108}Cd , ^{124}Sn , ^{128}Te , ^{130}Te , ^{136}Xe , and ^{150}Nd , *Nucl. Phys. A* **1042**, 122808 (2024).
- [13] K. Abe, K. Hiraide, K. Ichimura, Y. Kishimoto, K. Kobayashi *et al.*, Improved search for two-neutrino double electron capture on ^{124}Xe and ^{126}Xe using particle identification in XMASS-I, *Prog. Theor. Exp. Phys.* **2018**, 053D03 (2018).
- [14] J. Aalbers, D. S. Akerib, A. K. Al Musalhi, F. Alder, C. S. Amarasinghe *et al.* (The LUX-ZEPLIN Collaboration), Two-neutrino double electron capture of ^{124}Xe in the first LUX-ZEPLIN exposure, <https://arxiv.org/abs/2408.17391>.
- [15] A. P. Meshik, C. M. Hohenberg, O. V. Pravdivtseva, and Ya. S. Kapusta, Weak decay of ^{130}Ba and ^{132}Ba : Geochemical measurements, *Phys. Rev. C* **64**, 035205 (2001).
- [16] M. Agostini, A. Alexander, G. R. Araujo, A. M. Bakalyarov, M. Balata *et al.* (GERDA Collaboration), An improved limit on the neutrinoless double-electron capture of ^{36}Ar with GERDA, *Eur. Phys. J. C* **84**, 34 (2024).
- [17] M. Laubenstein, B. Lehnert, S. S. Nagorny, and S. Nisi, First search for resonant enhanced neutrinoless double electron capture in ^{152}Gd and other rare decays in natural Gd isotopes, *Eur. Phys. J. C* **83**, 1114 (2023).
- [18] K. Blaum, S. Eliseev, F. A. Danevich, V. I. Tretyak, S. Kovalenko *et al.*, Neutrinoless double-electron capture, *Rev. Mod. Phys.* **92**, 045007 (2020).
- [19] S. Bustabad, G. Bollen, M. Brodeur, D. L. Lincoln, S. J. Novario *et al.*, Examination of the possible enhancement of neutrinoless double-electron capture in ^{78}Kr , *Phys. Rev. C* **88**, 035502 (2013).
- [20] G. Martínez-Lema, M. Martínez-Vara, M. Sorel, C. Adams, V. Álvarez *et al.*, Sensitivity of the NEXT experiment to Xe-124 double electron capture, *J. High Energ. Phys.* **2021**, 203 (2021).
- [21] M. Pujol, B. Marty, P. Burnard, and P. Philippot, Xenon in Archean barite: Weak decay of ^{130}Ba , mass-dependent isotopic fractionation and implication for barite formation, *Geochim. Cosmochim. Acta* **73**, 6834 (2009).
- [22] D. S. Akerib, S. Alsum, H. M. Araújo, X. Bai, J. Balajthy *et al.*, Search for two neutrino double electron capture of ^{124}Xe and ^{126}Xe in the full exposure of the LUX detector, *J. Phys. G: Nucl. Part. Phys.* **47**, 105105 (2020).
- [23] J. Suhonen, Analysis of double- β transitions in ^{78}Kr , *Phys. Rev. C* **87**, 034318 (2013).
- [24] L. Pacearescu, V. Rodin, F. Šimkovic, and A. Faessler, Two-neutrino double β decay within fully renormalized quasiparticle random-phase approximation: Effect of the restoration of the Ikeda

- sum rule, Phys. Rev. C **68**, 064310 (2003).
- [25] M. S. Yousef, V. Rodin, A. Faessler, and F. Šimkovic, Two-neutrino double β decay of deformed nuclei within the quasiparticle random-phase approximation with a realistic interaction, Phys. Rev. C **79**, 014314 (2009).
- [26] J. Barea, and F. Iachello, Neutrinoless double- β decay in the microscopic interacting boson model, Phys. Rev. C **79**, 044301 (2009).
- [27] K. Nomura, Two-neutrino double- β decay in the mapped interacting boson model, Phys. Rev. C **105**, 044301 (2022).
- [28] P. K. Raina, A. Shukla, S. Singh, P. K. Rath, and J. G. Hirsch, The $0^+ \rightarrow 0^+$ positron double- β decay with emission of two neutrinos in the nuclei ^{96}Ru , ^{102}Pd , ^{106}Cd and ^{108}Cd , Eur. Phys. J. A **28**, 27 (2006).
- [29] J. Kostensalo, and J. Suhonen, Consistent large-scale shell-model analysis of the two-neutrino $\beta\beta$ and single β branchings in ^{48}Ca and ^{96}Zr , Phys. Lett. B **802**, 135192 (2020).
- [30] M. Horoi, S. Stoica, and B. A. Brown, Shell-model calculations of two-neutrino double- β decay rates of ^{48}Ca with the GXP1A interaction, Phys. Rev. C **75**, 034303 (2007).
- [31] J. Jia, H. Li, and C. Dong, Shell-model Study of Two-neutrino Double-Beta Decay for $Z = 40 - 50$ Nuclei and their SSD Properties, Phys. Scr. **98**, 025301 (2023).
- [32] J. Kostensalo, J. Suhonen, and K. Zuber, The first large-scale shell-model calculation of the two-neutrino double beta decay of ^{76}Ge to the excited states in ^{76}Se , Phys. Lett. B **831**, 137170 (2022).
- [33] E. Caurier, F. Nowacki, and A. Poves, Shell Model description of the $\beta\beta$ decay of ^{136}Xe , Phys. Lett. B **711**, 62 (2012).
- [34] B. A. Brown, D. L. Fang, and M. Horoi, Evaluation of the theoretical nuclear matrix elements for $\beta\beta$ decay of ^{76}Ge , Phys. Rev. C **92**, 041301(R) (2015).
- [35] L. Coraggio, N. Itaco, G. De Gregorio, A. Gargano, Z. H. Cheng *et al.*, The renormalization of the shell-model Gamow-Teller operator starting from effective field theory for nuclear systems, Phys. Rev. C **109**, 014301 (2024).
- [36] N. Shimizu, J. Menéndez, and K. Yako, Double Gamow-Teller Transitions and its Relation to Neutrinoless $\beta\beta$ Decay, Phys. Rev. Lett. **120**, 142502 (2018).
- [37] H. A. Bethe, Nuclear Physics B. Nuclear Dynamics, Theoretical, Rev. Mod. Phys. **9**, 69 (1937).
- [38] A. Gilbert, and A. G. W. Cameron, A Composite nuclear-level density formula with shell corrections, Can. J. Phys. **43**, 1446 (1965).
- [39] J. Kotila, and F. Iachello, Phase space factors for $\beta^+\beta^+$ decay and competing modes of double- β decay, Phys. Rev. C **87**, 024313 (2013).
- [40] J. Suhonen, Value of the Axial-Vector Coupling Strength in β and $\beta\beta$ Decays: A Review, Front. Phys. **5**, 55 (2017).
- [41] J. Suhonen, and O. Civitarese, Weak-interaction and nuclear-structure aspects of nuclear double beta decay, Physics Reports **300**, 123 (1998).
- [42] J. Suhonen, and O. Civitarese, Double-beta-decay nuclear matrix elements in the QRPA framework, J. Phys. G: Nucl. Part. Phys. **39**, 085105 (2012).
- [43] A. Hosaka, K.-I. Kubo, and H. Toki, G -matrix effective interaction with the paris potential, Nucl. Phys. A **444**, 76 (1985).
- [44] X. Ji, and B. H. Wildenthal, Effective interaction for $N = 50$ isotones, Phys. Rev. C **37**, 1256 (1988).
- [45] D. H. Gloeckner, Shell-model systematics of the zirconium and niobium isotopes, Nucl. Phys. A **253**, 301 (1975).
- [46] F. J. D. Serduke, R.D. Lawson, and D.H. Gloeckner, Shell-model study of the $N = 49$ isotones, Nucl. Phys. A **256**, 45 (1976).
- [47] P. Dey, D. Negi, R. Palit, P. C. Srivastava, Md. S. R. Laskar *et al.*, Experimental investigation of high-spin states in ^{90}Zr , Phys. Rev. C **105**, 044307 (2022).
- [48] G. Kumbartzki, N. Benczer-Koller, J. Holden, G. Jakob, T.J. Mertzimekis, Competition between

- proton and neutron excitations in ^{96}Zr , Phys. Lett. B **562**, 193 (2003).
- [49] A. E. Stuchbery, N. Benczer-Koller, G. Kumbartzki, and T. J. Mertzimekis, Gyromagnetic ratios and octupole collectivity in the structure of the $^{90-96}\text{Zr}$ isotopes, Phys. Rev. C **69**, 044302 (2004).
- [50] D. Patel, P. C. Srivastava, and J. Suhonen, Systematic shell-model analysis of $2\nu\beta\beta$ decay of ^{76}Ge and ^{96}Zr to the ground and excited states of ^{76}Se and ^{96}Mo , Phys. Rev. C **110**, 054323, (2024).
- [51] Evaluated Nuclear Structure Data File (ENSDF) <http://www.nndc.bnl.gov/ensdf/>.
- [52] B.A. Brown, and W.D.M. Rae, The Shell-Model Code NuShellX@MSU, Nucl. Data Sheets **120**, 115 (2014).
- [53] NuDat 3 - National Nuclear Data Center, https://www.nndc.bnl.gov/nudat3/indx_adopted.jsp.
- [54] N. Boelaert, N. Smirnova, K. Heyde, and J. Jolie, Shell model description of the low-lying states of the neutron deficient Cd isotopes, Phys. Rev. C **75**, 014316 (2007).
- [55] Y. Liu, S. Yu, and C. Shen, Structure of high spin state in proton-rich $^{74,76,78}\text{Kr}$ isotopes: A projected shell model description, Sci. China Phys. Mech. Astron. **58**, 1 (2015).
- [56] D. H. E. Gross, and R. Heck, What is wrong with the Bethe-formula for the nuclear level-density? measurable differences between grandcanonical and the microcanonical treatments, Phys. Lett. B **318**, 405 (1993).
- [57] A.J. Koning, S. Hilaire, and S. Goriely, Global and local level density models, Nucl. Phys. A **810**, 13 (2008).
- [58] T. Rauscher, F.-K. Thielemann, and K.-L. Kratz, Nuclear level density and the determination of thermonuclear rates for astrophysics, Phys. Rev. C **56**, 1613 (1997).
- [59] O. A. Rumyantsev, and M.H. Urin, The strength of the analog and Gamow-Teller giant resonances and hindrance of the $2\nu\beta\beta$ -decay rate, Phys. Lett. B **443**, 51 (1998).
- [60] P. F. Hinrichsen, G. Kennedy, and T. Paradellis, Level structure of ^{78}Se , Nucl. Phys. A **212**, 365 (1973).
- [61] S. K. L. Sjue, D. Melconian, A. García, I. Ahmad, A. Algora *et al.*, Electron-capture branch of ^{100}Tc and tests of nuclear wave functions for double- β decays, Phys. Rev. C **78**, 064317 (2008).
- [62] V. Kumar, and P. C. Srivastava, Shell-model study of β^+ /EC-decay half-lives for $Z = 21 - 30$ nuclei, Eur. Phys. J. A **59**, 237 (2023).
- [63] C. Patrignani, Review of Particle Physics, Chinese Phys. C **40**, 100001 (2016).
- [64] J. Suhonen, *From Nucleons to Nucleus: Concepts of Microscopic Nuclear Theory*, Springer, Berlin, 2007.
- [65] M. Haaranen, J. Kotila, and J. Suhonen, Spectrum-shape method and the next-to-leading-order terms of the β -decay shape factor, Phys. Rev. C **95**, 024327 (2017).